

A twisted and precessing Cepheid warp in the outer Milky Way disc

Walter Dehnen^{1,2,★}, Marcin Semczuk^{1,2} and Ralph Schönrich^{1,3}

¹*Astronomisches Rechen-Institut, Zentrum für Astronomie der Universität Heidelberg, Mönchhofstraße 12-14, D-69120 Heidelberg, Germany*

²*School for Physics and Astronomy, University of Leicester, University Road, Leicester LE1 7RH, UK*

³*Mullard Space Science Laboratory, University College London, Holmbury St Mary, Dorking, Surrey RH5 6NT, UK*

Accepted 2023 May 15. Received 2023 May 15; in original form 2023 April 13

ABSTRACT

We examine the Galactic warp in a sample of all classical Cepheids with *Gaia* Data Release 3 radial velocity. In each radial bin, we determine (1) the inclined plane normal to the mean orbital angular momentum of the stars and (2) that best fitting their positions. We find no warping inside $R \approx 11$ kpc; for larger R , the disc is increasingly inclined, reaching $i \sim 3^\circ$ at $R \geq 14$ kpc. With larger R , the azimuth of the warp’s ascending node shifts from $\phi_{\text{lon}} \approx -15^\circ$ at 11 kpc by about $14^\circ \text{ kpc}^{-1}$ in the direction of Galactic rotation, implying a leading spiral of nodes, the general behaviour of warped galaxies. From the method of fitting planes to the positions, we also obtain $\dot{\phi}_{\text{lon}}$ and find prograde precession of $\dot{\phi}_{\text{lon}} \sim 12 \text{ km s}^{-1} \text{ kpc}^{-1}$ at 12 kpc decreasing to $\sim 6 \text{ km s}^{-1} \text{ kpc}^{-1}$ at 14 kpc and beyond. This would unwind the leading spiral of nodes in ~ 100 Myr, suggesting that our instantaneous measurements of $\dot{\phi}_{\text{lon}}$ reflect transient behaviour. This is consistent with existing simulations, which show oscillations in $\dot{\phi}_{\text{lon}}$ overlaying a long-term retrograde differential precession that generates the leading spiral of nodes.

Key words: Galaxy: kinematics and dynamics – Galaxy: structure – Galaxy: disc – galaxies: spiral – stars: variables: Cepheids.

1 INTRODUCTION

At least half of all edge-on spiral galaxies appear to be warped (Sánchez-Saavedra, Battaner & Florido 1990; Bosma 1991; García-Ruiz, Sancisi & Kuijken 2002). Since a warp is not detectable from all edge-on orientations, this implies that in fact most disc galaxies are warped. The simplest model conceptualizes a warp as a sequence of nested rings in circular motion, each tilted with respect to the flat inner galaxy. Briggs (1990) fitted such tilted-ring models to the H I distribution of spiral galaxies and found that the warp typically begins near the Holmberg radius and reaches tilt angles of 5° – 20° , though values up to 90° (for polar-ring galaxies) also occur. As soon as an appreciable tilt is reached, its orientation can be measured, and Briggs (1990) found them to vary with radius such that the line of nodes forms a leading spiral (‘Briggs’ rule’).

The H I warp of the Milky Way is clearly visible in 21 cm emission (Burke 1957; Westerhout 1957; Henderson, Jackson & Kerr 1982). Using kinematic distances, Burton (1988) found it to commence at $R = 10$ kpc with increasing tilt (3° at 16 kpc, which for the Milky Way corresponds the Holmberg radius), but also to being lopsided outside 14.5 kpc (from Burton 1988 fig. 7.19 after correcting for his too large value for R_0). Whether or not the Galactic H I warp is twisted with a leading spiral of nodes, as for external galaxies, is difficult to assess, since (i) the lopsidedness complicates the picture and (ii) the line of nodes is close to the anticentre direction, where kinematic distances are unavailable. Burton (1988)’s analysis suggests a twist (in the same sense as seen in external galaxies) inside 14.5 kpc, while Levine, Blitz & Heiles (2006, also using kinematic distances)

concluded that the data are consistent with the line of nodes being in the anticentre direction at all radii.

The Milky Way warp is also manifest in the distribution of stars and dust across the sky (Djorgovski & Sosin 1989; Freudenreich et al. 1994; Drimmel & Spergel 2001; López-Corredoira et al. 2002; Reylé et al. 2009, among others), but for a quantitative analysis the distances to the tracers are required. Accurate astrometric parallax measurements only reach as far as 100 pc (*Hipparcos*) and 3–5 kpc (*Gaia*, depending on magnitude), i.e. the (extended) solar neighbourhood. None the less, the stellar warp has been identified in this region (Chrobáková, Nagy & López-Corredoira 2022), in particular through the variation of the mean vertical motion with position, from *Hipparcos* (Dehnen 1998; Drimmel, Smart & Lattanzi 2000) and more clearly from the *Gaia* data (Poggio et al. 2018; Schönrich & Dehnen 2018; Cheng et al. 2020; Poggio et al. 2020). For more extended studies of the stellar warp, less accurate photometric distances can be utilized (López-Corredoira et al. 2014; Romero-Gómez et al. 2019; Cheng et al. 2020; Li et al. 2020), but the large systematic distance uncertainties (e.g. from misclassification and extinction) risk bungling properties inferred for the warp. More recently, sufficiently large samples of Galactic Cepheids with accurate distances became available. These provide a wide view over the young stellar disc on our side of the Milky Way and clearly show the warp structure (Chen et al. 2019; Skowron et al. 2019a, b; Lemasle et al. 2022).

Most of these studies represent the mean vertical displacement of stars via an azimuthal Fourier series,

$$\bar{z}(R, \varphi) = Z_0 + Z_1 \sin(\varphi - \psi_1) + Z_2 \sin 2(\varphi - \psi_2) \quad (1)$$

with amplitudes Z_m and phases ψ_m that are functions of radius R . An inclined plane with inclination $i \ll 90^\circ$ produces an $m = 1$ component with amplitude $Z_1 = R \tan i$ and line of nodes $\varphi_{\text{lon}} = \psi_1$;

* E-mail: walter.dehnen@uni-heidelberg.de

$m = 0$ corresponds to an overall vertical offset of the disc and $m = 2$ corresponds to a saddle-shaped bend, rendering the warp lopsided. Many of the aforementioned studies restrict themselves to the $m = 1$ component, limit ψ_m to constants, and $Z_m(R)$ to simple functional forms. Their findings for the stellar warp agree reasonably well with those found for H I: the warp begins at ~ 11 kpc and reaches tilts of $\sim 3^\circ$ at 16 kpc with a line of nodes close to the anticentre direction, apparently without appreciable twist.

A somewhat more detailed analysis was performed by Chen et al. (2019), who in addition to a general fit of an $m = 1$ model split their sample of Cepheids into radial bins and fitted a tilted ring ($m = 1$) to each. They found the line of nodes to vary radially with $\varphi_{\text{lon}} \sim 0^\circ$ at 12.5 kpc and increasing to $\sim 20^\circ$ at $R > 14.5$ kpc,¹ thus forming a leading spiral and adhering to Briggs’ rule.

For a warp consisting of tilted rings in near-circular motion, hereafter termed ‘simple’ warp, (i) only the $m = 1$ component of the series (1) has significant amplitude and (ii) the warp undergoes nodal precession with rate $\dot{\psi}_1 = \Omega_p$, where $\Omega_p \equiv \Omega_\varphi - \Omega_z$ is the precession rate of individual stellar orbits (Ω_φ and Ω_z are the orbital frequencies for azimuthal rotation and vertical oscillation, respectively). For oblate systems $\Omega_\varphi \lesssim \Omega_z$, such that a simple warp precesses slowly backwards (retrograde) and, since $|\Omega_p|$ decreases outwards, differential precession naturally winds up the line of nodes into a leading spiral.

However, there are clear indications that the Milky Way warp is not simple. First, the H I distribution shows strong lopsidedness, implying a significant $m = 2$ component. Secondly, when interpreting the vertical stellar motions in terms of a simple warp model, Poggio et al. (2020) and Cheng et al. (2020) found precession rates of 10.9 and 13.6 km s^{−1} kpc^{−1} from samples of giants and the general stellar population, respectively, indicating fast prograde precession ($\Omega_\varphi \sim 20$ km s^{−1} kpc^{−1} at the relevant radii), instead of slow backward precession [note, though, that using similar analysis Wang et al. (2020) and Chrobáková & López-Corredoira (2021) found their data to be consistent with a static non-precessing warp]. All these studies combined highly uncertain astrometric parallaxes with photometric distances, which are known to be prone to systematic biases that dominate over the statistical uncertainties and are hard to quantify (Schönrich, Asplund & Casagrande 2011; Williams et al. 2013). When using Cepheids, these problems are much reduced and the errors largely limited to statistical uncertainties, which are larger due to smaller sample size, but fully quantifiable.

In this study of the Cepheid warp, we are improving on previous studies in several ways. First, we consider the distribution over the angular-momentum directions of the stars, i.e. their individual instantaneous orbital planes. This is similar to the pole-count map employed by Romero-Gómez et al. (2019) for OB and RGB star samples, except that we do not need to marginalize over the radial velocity, since these are known for all Cepheids in our sample. Secondly, we fit precessing tilted planes to the distributions of the Cepheids. The orientation of the respective planes is conventionally described in terms of their inclination i and the Galactocentric azimuth φ_{lon} of the line of nodes. In case of the tilted planes fitted to the Cepheid positions, we also obtain the time derivatives of these, i.e. di/dt and the precession rate $\dot{\varphi}_{\text{lon}}$. These measurements for the

precession rate are superior to those from previous studies, since (i) Cepheid distances are much more accurate (at the relevant radii), (ii) no assumption is made regarding the stationarity of the warp (previous studies implicitly assumed $di/dt = 0$), and (iii) we do this over bins in guiding-centre radius R_g , thereby obtaining radial profiles for all these quantities.

This paper is organized as follows: In Section 2, we present the Cepheid sample, which we analyse in various ways in Section 3. Finally, in Section 4 we discuss our findings and conclude in Section 5.

2 THE DATA

2.1 Cepheid characteristics

We now briefly summarize some properties of Cepheids that have some relevance in the present context, but may not all be well known to our readers. Most Cepheids begin their life as B-type main-sequence stars. When such a star has become a red giant (or even before it gets there), it ignites helium in the core and may perform a ‘blue loop’ in the Hertzsprung–Russell diagram. On this loop, it passes the instability strip on its way to higher temperatures and again on its way back to the asymptotic giant branch.

Whether a star undergoes such a blue loop and how long it takes depend sensitively on its mass, metallicity, and helium abundance. At near-solar metallicities, stars with masses of 4.5–10 M_⊙ will become Cepheids (Anderson et al. 2014), while at sub-solar metallicities this range becomes 3–12 M_⊙, i.e. reaching into A-type stars. This metallicity dependence has two consequences. First, Cepheids are more abundant in metal-poor populations (owing to the scarcity of higher mass stars) such as in the Small Magellanic Cloud, and in the Milky Way disc their fraction increases outwards. Secondly, metal-poor Cepheids are on average fainter and older than metal-rich Cepheids.

How long a star lives before its blue loop depends sensitively on its rotation (Anderson et al. 2016), with fast rotators taking almost twice as long. Since binarity can sustain the initial fast rotation of B stars, and Cepheids are often found to be binary (Kervella et al. 2019), single-star evolutionary tracks may significantly underestimate their true age.

2.2 The sample

We use the sample of Milky Way Classical Cepheids presented by (Gaia Collaboration 2022a, hereafter G22) that consists of Cepheids identified (Ripepi et al. 2022a) in *Gaia* Data Release (DR) 3 (Gaia Collaboration 2022b) as well as those from the catalogues of Inno et al. (2021) and Pietrukowicz, Soszyński & Udalski (2021). It combines EDR3 astrometry (position, proper motion; Lindegren et al. 2021) and DR3 radial velocities with distances obtained from the Classical-Cepheid period–luminosity relation (Ripepi et al. 2019, 2022b) to obtain the full 3D kinematics for 2123 stars.² We follow Semiczek et al. (2023) and adopt for the velocity of the Sun (needed to convert to Galactocentric phase-space coordinates)

$$\mathbf{v}_\odot = (13, 250, 6.9) \text{ km s}^{-1}, \quad (2)$$

¹Chen et al. (2019) also found φ_{lon} to increase inwards from 12.5 kpc (forming a trailing spiral), where the tilt is generally small. However, this result is less reliable, because at such small inclinations the best-fitting tilted ring is more strongly affected by dust obscuration. While not reflected in their error bars, this makes the line of nodes highly uncertain.

²Adding near-infrared detected Cepheids can in theory extend the sample to behind the Galactic centre, providing a much wider view of the Milky Way disc. However, as the danger of confusing spotted stars for Cepheids is substantial (Pietrukowicz et al. 2015), we refrain from such an extension to keep a homogeneous sample.

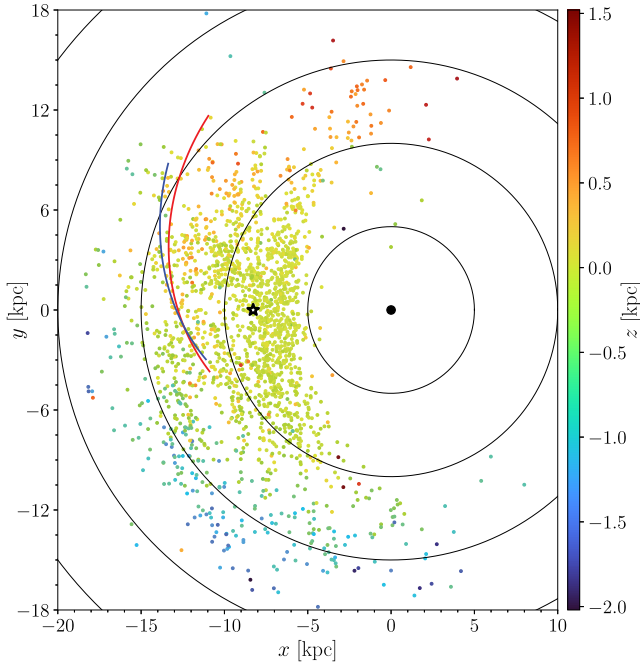


Figure 1. The distribution in the Galactic plane (the Sun and Galactic centre are indicated; Galactocentric circles differ by 5 kpc in radius) of the 2009 Classical Cepheids analysed (excluding 114 high-eccentricity stars; see the text). Colour indicates vertical position (clipped to $[-2, 1.5]$ kpc). The arcs indicate the twisting line of nodes of the warp as found from our analyses of the Cepheid’s orbital planes (red) and positions (blue).

which is a blend of the results derived by Schönrich, Binney & Dehnen (2010) and Schönrich (2012) and deviates from that adopted by Gaia Collaboration (2022a). As these values are not very well known (systematics dominate over uncertainties) and affect our analysis, we will explore the effect of different values. Similarly, we explore the effect of an alternative Cepheid period–luminosity relation (Cruz Reyes & Anderson 2023).

The sample contains some stars on significantly non-circular orbits, which could be artefacts of erroneous distance (due to misclassification of a non-Cepheid) and/or radial velocity or could be caused by the kick suffered when a supernova explodes in a binary (of which the Cepheid progenitor was the secondary). Whatever the cause, eccentric orbits are also likely to be randomly inclined and hence no good tracers of any warp. We therefore remove stars with orbital eccentricity $e > 0.2$, defined as the ratio between the epicycle amplitude and the radius of the guiding-centre orbit. We compute e using the epicycle approximation as (see Binney & Tremaine 2008, equations 3.98 and 3.99)

$$e = \frac{\gamma}{2v_{\text{circ}}} [\gamma^2(v_t - v_{\text{circ}})^2 + v_r^2]^{1/2}. \quad (3)$$

Here, $\gamma = 2\Omega/\kappa$ with Ω and κ the tangential and radial epicycle frequencies, v_t and v_r are the star’s tangential and radial velocity, respectively, and v_{circ} is the speed of the circular orbit with the same total angular momentum as the star. We assume a flat circular speed curve with $v_{\text{circ}} = 238 \text{ km s}^{-1}$, when $\gamma = \sqrt{2}$. This procedure removes 114 stars such that 2009 remain (our findings are insensitive to the precise value of the eccentricity cut-off or the assumption of a flat circular-speed curve, as demonstrated in Section 3.3).

In Fig. 1, we plot the distribution of these stars in the Galactic plane, indicating in colour their vertical offset from the mid-plane (as defined by Galactic latitude $b = 0$).

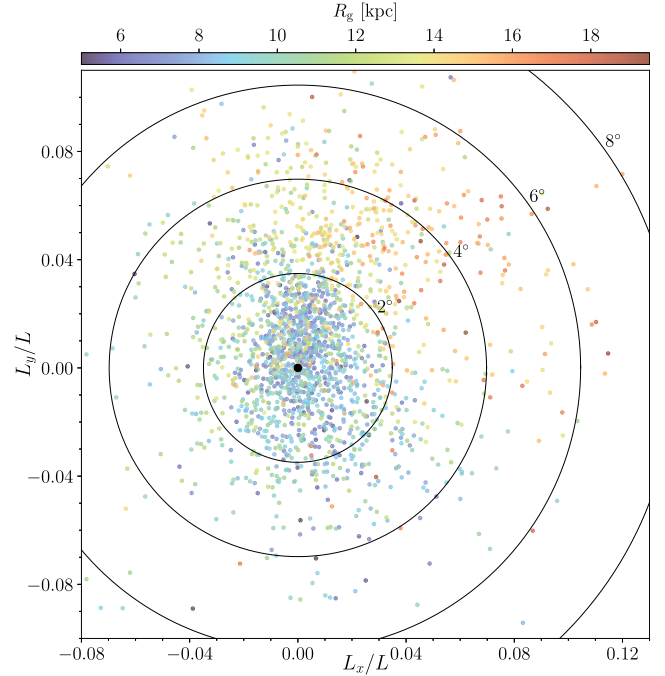


Figure 2. The distribution of Galactic Cepheids from Fig. 1 over the x and y components of the directions $\hat{\mathbf{L}}$ of angular momentum. Colour indicates the guiding-centre radius of their orbit. A value of $(\hat{L}_x, \hat{L}_y) = (0, 0)$ (black dot) corresponds to alignment with Galactic coordinates, while circles indicate tilts of 2° , 4° , 6° , and 8° .

As the Cepheids in the outer disc are generally metal poor compared to the Sun, they are also less massive (as explained above) and older. The ages estimated by G22 for this sample range between 100 Myr for Cepheids near the Sun to about 200 Myr in the outer disc, although the true ages may well be up to twice as large owing to binarity, as explained earlier.

3 ANALYSIS

The Galactic warp is clearly visible in Fig. 1 as a systematic vertical displacement of the stars. Several recent studies of similar samples of Galactic Cepheids (Chen et al. 2019; Skowron et al. 2019a, b; Lemasle et al. 2022) have analysed solely their spatial distribution and done so predominantly by fitting a parametrized radial warp profile. Here, we improve on these studies by (i) including the velocities in our analysis and (ii) performing it in radial bins (non-parametric).

A better estimate for a star’s typical radial position than its instantaneous radius is the guiding-centre radius R_g of its orbit, i.e. the radius of a circular orbit with the same angular momentum. We split the sample into 22 bins in R_g (computed using the same model for v_{circ} as for the eccentricity cut) with the same number of stars per bin, and also consider the 21 intermittent bins between the medians of these primary bins, resulting in 43 bins in total.

3.1 Instantaneous orbital planes

Adding the velocities \mathbf{v} to the positions \mathbf{x} enables the computation of the angular momenta $\mathbf{L} = \mathbf{x} \times \mathbf{v}$ and hence of the instantaneous orbital planes perpendicular to \mathbf{L} . The unit vector $\hat{\mathbf{L}} = \mathbf{L}/|\mathbf{L}|$ defines for each star the unit *normal* to or *pole* of its instantaneous orbital plane. In Fig. 2, we plot the distribution of the projection of these

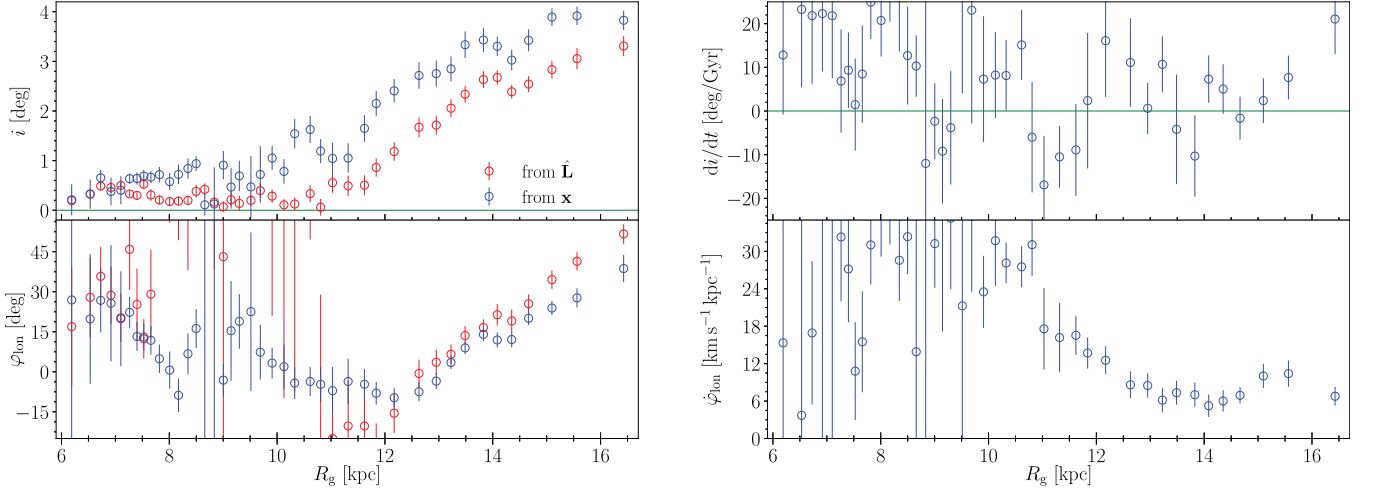


Figure 3. Left: Tilt (inclination) i (top) and azimuth φ_{lon} of the line of nodes (bottom, defined to be 0° for the position of the Sun and increasing in direction of Galactic rotation) for Cepheids in 43 bins in guiding-centre radius R_g . The red points are obtained from the mean angular-momentum directions $\langle \hat{\mathbf{L}} \rangle$, while the blue points are obtained by fitting an inclined plane to the positions only. The large noise and uncertainties for φ_{lon} at small R_g reflect the fact that φ_{lon} is ill-determined for small inclination. Right: The rate of change di/dt of the tilt (inclination, top) and the precession rate $\dot{\varphi}_{\text{lon}}$ for the inclined planes fitted to the Cepheids position in each of 43 bins in guiding-centre radius R_g .

poles on to the x - y plane (equivalent to pole-count maps or great-circle cell counts; Johnston, Hernquist & Bolte 1996). Stars whose orbital plane is aligned with the Galactic coordinates would be at the origin in this plot, while $\hat{\mathbf{L}}$ on circles around the origin are inclined by the same degree, but in different directions.

In Fig. 2, we colour code the stars according to R_g . Stars at small R_g cluster more around $\hat{\mathbf{L}} = 0$, reflecting a flat inner disc, while stars at larger R_g tend to have $\hat{\mathbf{L}}_y > 0$, indicative of the warp. In each of the 43 R_g bins, we compute the mean $\langle \hat{\mathbf{L}} \rangle$,³ which corresponds to a mean inclination and a mean azimuth for the line of nodes, which we plot in the left-hand panels of Fig. 3 (red circles) against the median guiding-centre radius for each bin. At $R_g \lesssim 11$ kpc, the angular momenta of the Cepheids are on average close to being aligned with the Galactic south pole. The orbital planes of most stars in this inner part of the disc are inclined by $\lesssim 1^\circ$ but in different directions with some preference for $\varphi_{\text{lon}} \sim 0^\circ$ ($\hat{\mathbf{L}}_y > 0$) and to a lesser degree $\sim 180^\circ$. In other words, the inner disc at $R_g \lesssim 11$ kpc does not show a coherent warp, but possibly a more complex picture (including a bent of the disc or a lopsided warp). The situation is further complicated by possible systematic errors in the assumed solar velocity and dust obscuration. We therefore refrain from a further analysis of the Cepheid warp at $R_g \lesssim 11$ kpc.

At $R_g \gtrsim 11$ kpc, on the other hand, the inclination increases quickly to 3° at 14 kpc and appears to stay at that level towards larger radii, although our sample does not probe much beyond $R_g = 16$ kpc.

In this inclined outer part of the Cepheid disc, we can also measure the orientation of the warp as described by the azimuth φ_{lon} of the ascending nodes, shown in the bottom left panel of Fig. 3. We find that φ_{lon} is in fact not constant, but increases with guiding-centre radius. This is in contrast to the usual modelling of the Cepheid warp in previous studies, all of which assume a single value (often set to $\varphi_{\text{lon}} = 0^\circ$). φ_{lon} increasing with radius corresponds to a twisting

warp with a leading spiral of nodes, which we indicate as red arch in Fig. 1. We find that the dependence is very well described by a simple linear increase and hence naturally described by its gradient $d\varphi_{\text{lon}}/dR_g$. In the remainder of this study, we refer to this gradient as the *twist* of the warp.

3.2 Fitting inclined planes

As our sample has no Cepheids behind the Galactic centre, and hence does not fully cover all azimuths, we cannot reliably distinguish the $m = 1$ and $m = 2$ Fourier components as defined in equation (1). Instead, we fit for each bin in R_g a precessing inclined plane (which for small inclination corresponds to the $m = 1$ Fourier component) to the Cepheids' Galactocentric directions $\hat{\mathbf{x}} = \mathbf{x}/|\mathbf{x}|$ and their time derivatives. To this end, we first find $\mathbf{a} \equiv \{a_x, a_y\}$ that minimizes

$$\chi^2 = \sum_i (a_x \hat{x}_i + a_y \hat{y}_i - \hat{z}_i)^2, \quad (4)$$

which is $\mathbf{a} = \mathbf{A}^{-1} \cdot \mathbf{b}$ with matrix $\mathbf{A} = \sum_i \{\hat{x}_i, \hat{y}_i\} \otimes \{\hat{x}_i, \hat{y}_i\}$ (\otimes denotes the outer product) and vector $\mathbf{b} = \sum_i \hat{z}_i \{\hat{x}_i, \hat{y}_i\}$. Secondly, we obtain the normal to the inclined plane as $\hat{\mathbf{n}} = \{a_x, a_y, -1\}(a_x^2 + a_y^2 + 1)^{-1/2}$. Thirdly, we compute $\hat{\mathbf{A}}$ and $\hat{\mathbf{b}}$ from the velocities and obtain $\hat{\mathbf{a}} = \hat{\mathbf{A}}^{-1} \cdot (\hat{\mathbf{b}} - \hat{\mathbf{A}} \cdot \hat{\mathbf{a}})$. Finally, the inclination and azimuth of the line of nodes are obtained as $i = \cos^{-1} |\hat{n}_z|$ and $\varphi_{\text{lon}} = \tan^{-1}(\hat{n}_x/\hat{n}_y) = \tan^{-1}(a_x/a_y)$, respectively, and their time derivatives by straightforward differentiation.

3.2.1 Inclination and line of nodes

In Fig. 4, we plot for four distinct bins in R_g (increasing from top to bottom) the distributions over $\hat{\mathbf{L}}_x$, $\hat{\mathbf{L}}_y$ (as in Fig. 2) in the left-hand panels, while the right-hand panels show the corresponding individual orbital planes (grey curves) projected on to Galactocentric azimuth and latitude (such that the Sun is at the origin and rotation to the right). These orbital planes show a clear and coherent warp, which is in good agreement with the spatial distribution (dots), at least at $R_g \gtrsim 12$ kpc. We show in red the average orbital plane (in the sense of the average $\langle \hat{\mathbf{L}} \rangle$) and in blue the inclined plane fitted to the normalized positions. In left-hand panels of Fig. 3, we also plot

³In practice, we compute the means of $\hat{\mathbf{L}}_x$ and $\hat{\mathbf{L}}_y$, whereby recursively ignoring stars outside of 3σ from the sample mean, though our findings are not sensitive to this κ - σ clipping. The mean of $\hat{\mathbf{L}}_z$ is then constructed from the normalization condition.

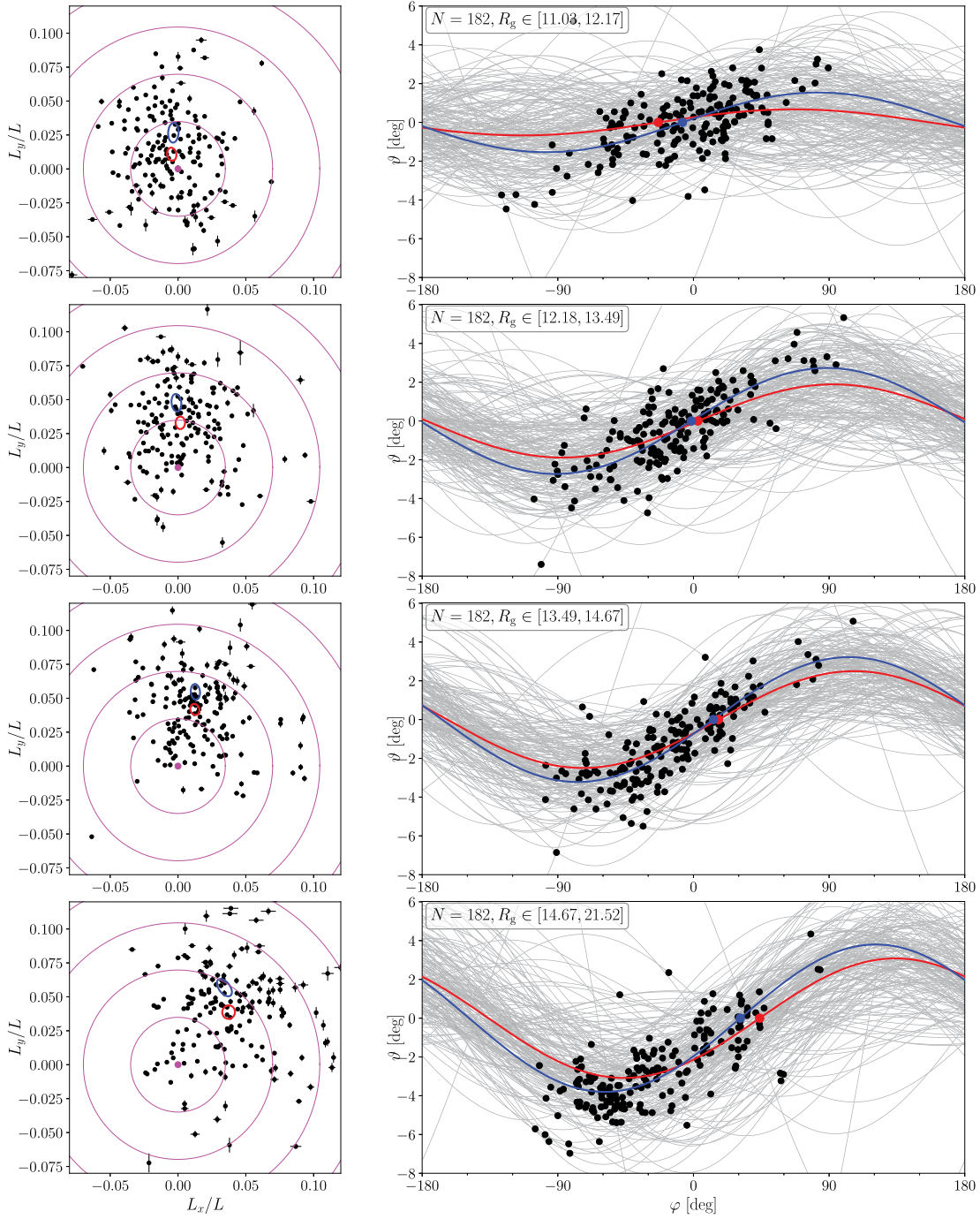


Figure 4. Warp for Cepheids in four distinct bins with increasing (from top to bottom) guiding-centre radius R_g , as indicated in the legends (each of these bins combines two of the 22 bins used for analysis). The left-hand panels are like Fig. 2, but include individual error bars. The right-hand panels show the spatial distribution of Cepheids (dots) over Galactocentric azimuth φ and latitude θ (in these coordinates, the Sun is at the origin and rotation to the right) and for each the projection of its instantaneous orbital plane (grey). The mean \vec{L} is indicated in the left-hand panels as 2σ (86 per cent) confidence region (red) and in the right-hand panels as projection of the normal plane (red). Similarly, the blue error ellipse (left-hand panel) and curve (right-hand panel) reflect the tilted plane that best fits the Cepheid positions.

(blue) the tilt (inclination i) and direction φ_{lon} of the line of nodes for the fitted inclined planes.

The inclined planes fitted to the positions are generally slightly more inclined than the average of the individual orbital planes. This could be (partly) caused by observational biases (since obscuration by dust hides some stars at low $|z|$) or be a real effect.

3.2.2 Tumble and precession

In the right-hand panels of Fig. 3, we plot the rates di/dt and $d\varphi_{\text{lon}}/dt$ against R_g . At $R_g \lesssim 11$ kpc, the warp amplitude is too small for reliably measuring these rates (resulting in large scatter and uncertainties). The rates of change of the inclination are consistent

Table 1. Dependence of the results for the twist $d\varphi_{\text{lon}}/dR_g$ and the precession rate $\dot{\varphi}_{\text{lon}}$ at $R_g = 12$ and 14 kpc (from bins with 100 Cepheids on either side of these) on eccentricity cut, the κ - σ clipping, the assumed solar velocity, the number of bins, the assumed rotation curve, and the Cepheid P - L relation. Values/methods not mentioned in the first column are at default (see Section 2).

Deviation from default	$d\varphi_{\text{lon}}/dR_g$ (deg kpc $^{-1}$)		$\dot{\varphi}_{\text{lon}}$ (km s $^{-1}$ kpc $^{-1}$)	
	from \hat{L}	from \hat{x}	at $R_g = 12$ kpc	at $R_g = 14$ kpc
Default [$v_{\odot} = (13, 250, 6.9)$ km s $^{-1}$, $e_{\text{max}} = 0.2$]	14.7 ± 0.7	10.6 ± 0.8	12.4 ± 1.6	5.9 ± 1.3
Maximum eccentricity $e_{\text{max}} = 0.1$	15.4 ± 1.0	11.6 ± 1.2	12.7 ± 1.5	6.1 ± 1.0
Maximum eccentricity $e_{\text{max}} = 0.3$	14.6 ± 0.7	10.5 ± 0.9	13.1 ± 1.7	6.2 ± 1.3
Using 44/87 primary/total bins	14.1 ± 0.7	10.4 ± 0.7	—	—
No κ - σ clipping to find $\langle \hat{L} \rangle$	14.9 ± 0.7	—	—	—
$v_{\odot} = (9.3, 251, 8.6)$ km s $^{-1}$ (G22)	13.0 ± 0.7	10.7 ± 0.8	8.9 ± 1.7	3.9 ± 1.4
$v_{\odot,z} = 8.6$ km s $^{-1}$	13.6 ± 0.6	10.7 ± 0.8	8.9 ± 1.6	3.7 ± 1.4
$v_{\odot,R} = 9.3$ km s $^{-1}$	14.3 ± 0.8	10.9 ± 0.8	12.0 ± 1.6	6.1 ± 1.3
$v_{\odot,\varphi} = 246$ km s $^{-1}$	14.3 ± 0.7	11.2 ± 0.9	10.8 ± 1.5	6.0 ± 1.2
$v_{\odot,\varphi} = 254$ km s $^{-1}$	15.2 ± 0.9	10.4 ± 1.0	14.7 ± 1.7	7.0 ± 1.3
$v_{\text{circ}} = 238$ km s $^{-1}$ (R/R_0) $^{-0.05}$	14.0 ± 0.6	10.1 ± 0.8	14.3 ± 1.8	6.5 ± 1.2
Cepheid P - L relation from Cruz Reyes & Anderson (2023)	14.9 ± 0.8	10.6 ± 0.9	12.4 ± 1.5	5.9 ± 1.3

with zero for most of the bins, except perhaps the marginally significant positive value for the outermost bin.

The precession rates, however, clearly show fast prograde precession, with $\dot{\varphi}_{\text{lon}} \approx 12$ km s $^{-1}$ kpc $^{-1}$ at $R_g = 12$ kpc, decreasing to ~ 6 km s $^{-1}$ kpc $^{-1}$ at $R_g \gtrsim 13$ kpc. This is in clear contradiction to the slow retrograde precession expected for a simple warp, but the former of these values is in good agreement with previous estimates for the general stellar population (Cheng et al. 2020; Poggio et al. 2020), which mainly probes $R \sim 12$ kpc. Our measurements at $R_g \gtrsim 13$ kpc are significantly smaller, but still positive and inconsistent with the expectation of a simple warp.

3.3 Effects of the solar velocity and other parameters

We repeated the analyses leading to Fig. 3 for twice the number of (primary) bins in R_g , no κ - σ clipping for finding $\langle \hat{L} \rangle$, as well as various deviating choices of the solar velocity, the threshold for the eccentricity cut, the assumed circular speed curve (affecting eccentricity e and guiding-centre radius R_g), and the Cepheid period-luminosity relation. For the latter, we explored the recent relation by Cruz Reyes & Anderson (2023), which is based on the metallicity-effect calibration by Breuval et al. (2022). For v_{\odot} , we explored the values adopted by Gaia Collaboration (2022a), either for all components or for the radial and vertical component only (which have the strongest effect).

The resulting profiles (not shown) for inclination i , line-of-node orientation φ_{lon} , and their time derivatives are largely similar to those obtained from our default values shown in Fig. 3, including the onset of the warp at $R_g \approx 11$ kpc, the typical inclination of $i = 3$ – 4 deg in the outer disc, and the fact that i found from orbital-plane analysis is generally $\sim 1^\circ$ smaller than that found from fitting a single plane to all Cepheids in a given R_g bin. The largest variation is found in the orientations φ_{lon} of the outer disc and its rate of change $\dot{\varphi}_{\text{lon}}$, as summarized in Table 1. Generally, the twist $d\varphi_{\text{lon}}/dR_g$ is 10–11 deg kpc $^{-1}$ for the single-plane fits and 13–15 deg kpc $^{-1}$ for the average orbital plane, with statistical uncertainties $\lesssim 1$ deg kpc $^{-1}$.

Obviously, different assumptions for the solar velocities have the strongest effect on $d\varphi_{\text{lon}}/dR_g$ obtained from $\langle \hat{L} \rangle$ and on the precession rates $\dot{\varphi}_{\text{lon}}$, both of which depend on the Cepheid velocities. Assuming a larger radial and/or smaller vertical velocity for the Sun (as did G22) reduces both of these measures with the strongest effect on $\dot{\varphi}_{\text{lon}}$ at $R_g = 12$ kpc. However, while the changes are

significant (larger than the statistical uncertainties), they are not substantial: the twist inferred from the individual orbital planes is still larger than that obtained from an inclined-plane fit and the precession remains fast and prograde. These results are hence robust.

4 DISCUSSION

4.1 Comparison to other studies

Fig. 5 compares our results (as already presented in earlier figures) to previous studies of the inclination and line of nodes of the Cepheid warp, as well as for precession rate of the general stellar warp. Our results largely agree with those previous studies, but our analysis provides a more detailed view, mainly owed to our binning of the Cepheid in guiding-centre radius R_g as opposed to an overall fit of a global model. The only previous exception to this global-fit approach was an analysis using radial bins by Chen et al. (2019), which allowed them to measure the radial change of the line of nodes (green triangles in the middle panel of Fig. 5). Their result agrees mostly with ours in the sense that the line of nodes forms a leading spiral at $R \gtrsim 12$ kpc, but we find the linear increase of φ_{lon} with radius to continue all the way to our outermost data point at 16 kpc, while Chen et al. (2019) find it to remain constant for $R \gtrsim 14$ kpc. Since our Cepheid sample extends further than that used by Chen et al. (2019), our result appears more reliable.

Previous estimates (Cheng et al. 2020; Poggio et al. 2020; Wang et al. 2020; Chrobáková & López-Corredoira 2021) for the warp precession rate have been obtained from general stellar samples using distance information that was (at least partly) based on astrometric parallaxes with rather low accuracy and by assuming that the warp is a coherently precessing (but otherwise unevolving) inclined disc with the same orientation (φ_{lon}) and precession ($\dot{\varphi}_{\text{lon}}$) at all radii. None of these assumptions is made by our analysis, which allows the inclination of the warp to vary with time and its orientation and precession rate with radius. Moreover, while the Cepheids sample is much smaller than the large samples used in those previous studies, their distances are excellent, preventing biases from distance systematics. Our measurements of $\dot{\varphi}_{\text{lon}}$ (bottom panel of Fig. 5) show a fast and radially decreasing precession, consistent with the previous estimates by Cheng et al. (2020) and Poggio et al. (2020), but not with those of Wang et al. (2020) and Chrobáková & López-Corredoira (2021), who found $\dot{\varphi}_{\text{lon}} \sim 0$. It is not entirely clear what drives these

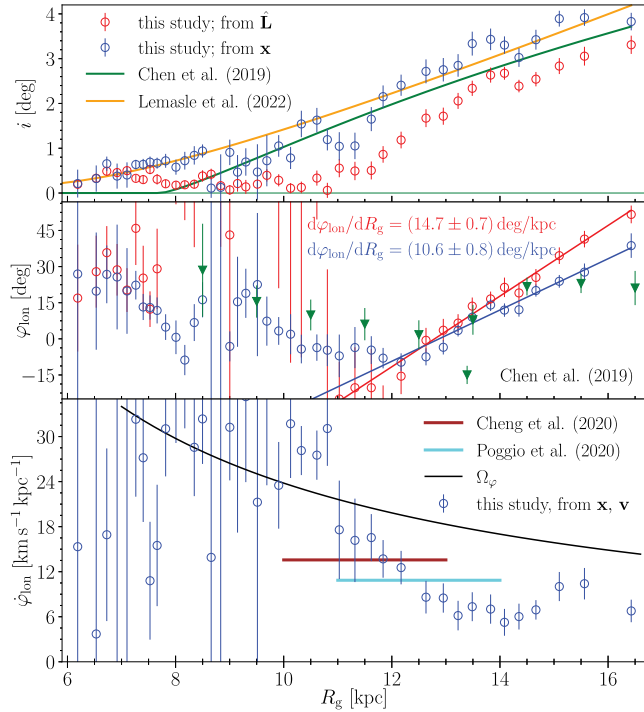


Figure 5. The results from this study obtained by analysing the Cepheids’ orbital planes (red circles) or fitting a precessing inclined plane (blue circles) to their positions and velocities are compared to previous studies of the Cepheid warp (Chen et al. 2019; Lemasle et al. 2022) and the warp precession rate inferred from the vertical proper motion of giants (Poggio et al. 2020) or the general stellar population (Cheng et al. 2020). As these latter two studies considered a single value for the precession rate at all radii (and also $\varphi_{\text{lon}} = 0^\circ$), we show their result over a radial range where the respective data sets carry most warp signal. We also plot Ω_φ for an assumed flat rotation curve.

differences (also between those previous studies),⁴ but as our method is based on accurate distances and involves no model assumptions, it is more reliable than any of these previous estimates.

After submission of our work, we became aware of a preliminary analysis by Cabrera-Gadea et al. (in preparation) of the Cepheid warp (albeit without using radial velocity information) with similar findings to ours regarding the twist and precession.

4.2 Where does the Cepheid warp start?

For each bin in guiding-centre radius R_g , we find a tilted plane describing the Cepheid warp in two different ways: as that normal to the mean angular momentum direction and by fitting to the positions (see Fig. 5). The resulting tilt angles, in particular those obtained by the fits, agree well with those found in previous studies of the Cepheid warp (Chen et al. 2019; Skowron et al. 2019a, b; Lemasle et al. 2022), as expected. The tilt angles obtained from the average orbital planes are generally smaller by about 1° . This could be at least partly caused by dust hiding Cepheids in the Galactic mid-plane, such that our sample is biased towards those warped out of the plane. We suspect that this mechanism is responsible for the

measured inclination of $\sim 1^\circ$ at $R_g \lesssim 11$ kpc, where the orbital-plane analysis suggests a flat disc instead. This is akin to the situation with Galactic OB stars, whose velocities are well described by dynamic equilibrium models but not their positions, which is best explained by unknown dust obscuration (Li & Binney 2022).

If this explanation is correct, it implies that the Cepheid warp actually begins at about 11 kpc and that any previously detected Cepheid warp inside that radius is an artefact of selection effects caused by dust obscuration.⁵ This would also imply that any measurements for the line of nodes in this region are invalid, such as the trailing spiral, also reported by Chen et al. (2019, shown by green triangles in the middle panel of Fig. 5 and consistent with our measurements).

4.3 The warp line of nodes

Another clear difference between the warp parameters obtained from the two methods is the twist of the line of nodes, which for the orbital-plane analysis is stronger (larger $d\varphi_{\text{lon}}/dR_g$). Apart from dust obscuration discussed earlier, there are other possible reasons for such differences. Even if the Cepheids are distributed in tilted rings, their angular momenta may well deviate from the normal to that ring, already because of the nodal precession. If the Cepheid warp is lopsided (like the H I warp), more deviations are expected, which may also depend on azimuth, of which our sample covers only half of the full range, as Cepheids on the other side of the Milky Way are hidden by dust.

Such deviations between these two different analysis methods are actually common for simulated galaxies. We applied our methods to Cepheid tracers (star particles younger than 300 Myr) in several simulated spiral galaxies of the IllustrisTNG (TNG50; Nelson et al. 2019; Pillepich et al. 2019) simulation and found a variety of behaviours, including a case that is similar to the Milky Way (shown in Fig. 6) with regard to the behaviour of $d\varphi_{\text{lon}}/dR_g$.

4.4 The warp precession rate

The line of nodes of the Cepheid warp, being a leading spiral, adheres to Briggs’ rule, i.e. behaves as most warped galaxies do and indeed also all simulated galactic warps in TNG50 that we analysed. The standard theoretical explanation, as already mentioned in the introduction, is that the warp precesses slowly in a retrograde sense with the orbital precession rate, i.e. $\dot{\varphi}_{\text{lon}} = \Omega_\varphi - \Omega_z$, when faster precession at smaller radii results in a leading spiral. And indeed, of the simulated warped galaxies in TNG50 for which we checked this, all adhere to this explanation, at least in the sense that our measurement for $\dot{\varphi}_{\text{lon}}$ mostly obtains negative values at 0–10 km s^{-1} , including the example presented in Fig. 6. However, our measurements for the Cepheids do not follow this trend, but instead obtain $\dot{\varphi}_{\text{lon}} > 0$. Moreover, the radial decline (from 12 to 6 $\text{km s}^{-1} \text{ kpc}^{-1}$ between 12 and 14 kpc) would wind the line of nodes into a *trailing* spiral or, equivalently, unwind the observed leading spiral in only ~ 100 Myr.

This contradiction implies immediately that the instantaneous $\dot{\varphi}_{\text{lon}}$ that we (and others) have measured cannot be the predominant warp precession rate for most of the history of the warp.

⁴Chrobáková & López-Corredoira (2021) claim that unsuitable warp parameters used by Poggio et al. (2020) invalidate their result, but Cheng et al. (2020) fitted those parameters to the kinematics and found essentially the same result.

⁵This suggestion is corroborated by our (preliminary) analysis of simulated warped galaxies in the TNG50 simulations, as we did not find a single one for which the orbital-plane analysis obtains $i \sim 0^\circ$ while the plane fitting gives $i \gtrsim 1^\circ$, as we found for the Milky Way inside ~ 11 kpc.

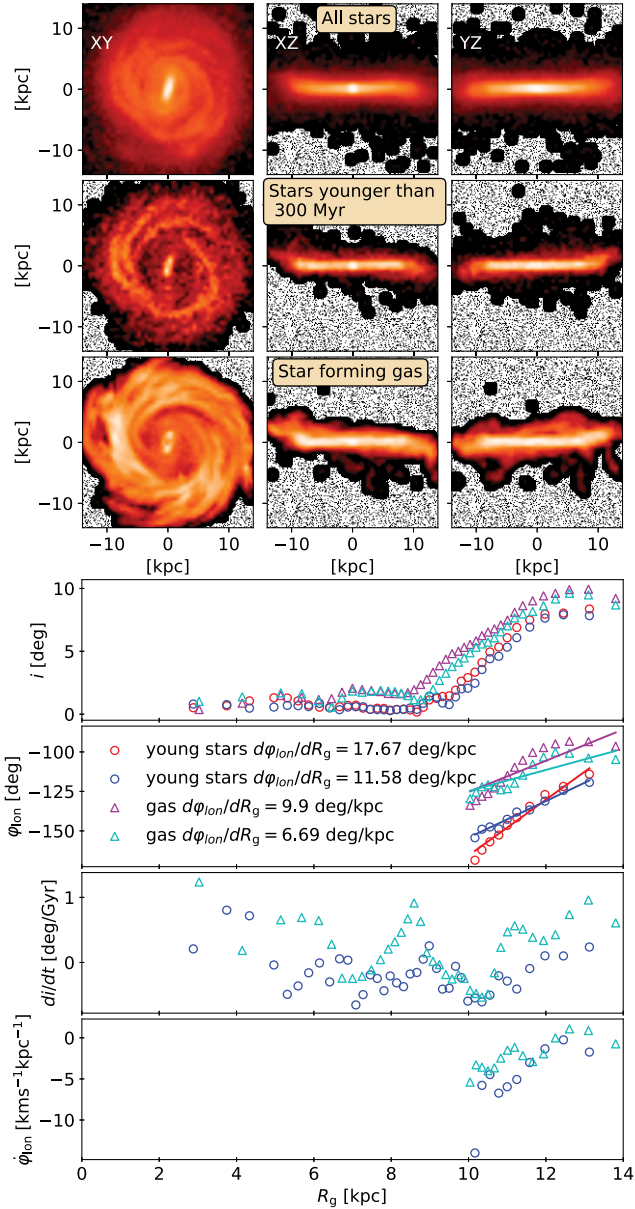


Figure 6. Projected density (top) and warp parameters (bottom) determined for young star particles and star-forming gas of a simulated spiral (galaxy ID 566365 at $z = 0$ of run TNG50-1) in the same ways as for the Milky Way Cepheids (red/purple symbol refers to the analysis of orbital angular momenta, while blue/cyan refers to inclined planes fitted to the positions).

A warp may in fact be a superposition of several bending waves with azimuthal wavenumber m , as stipulated in equation (1). In this case, each mode precesses with rate

$$\dot{\psi}_m \equiv \omega_m = \Omega_\phi \pm \frac{1}{m} \Omega_z, \quad (5)$$

where the ‘+’ sign obtains a fast and the ‘−’ sign a slow wave (see Binney & Tremaine 2008, chapter 6.6). The fast waves tend to wind up quickly such that eventually only the slowest survives, which is the slow $m = 1$ wave (‘simple’ warp), which precesses with the same rate as stellar orbits. However, lopsidedness (as observed for the Milky Way H I warp, but not easily detectable for Cepheids and other stellar samples due to the limited azimuthal coverage),

requires an $m = 2$ mode. In fact, the slow $m = 2$ mode precesses with $\Omega_\phi - \frac{1}{2}\Omega_z \sim \frac{1}{2}\Omega_\phi$, close to our measurement for $\dot{\phi}_{\text{lon}}$.

Previous studies estimated the precession rate assuming that the warp is an $m = 1$ wave. Our method of fitting an inclined plane, while allowing for a change of warp amplitude, also ignores lopsidedness ($m = 2$). However, as all of the available samples have rather limited azimuthal coverage, these modes cannot (currently) be easily disentangled. Instead, all these various analyses essentially measure the local propagation rate $\dot{\phi}_{\text{lon}}$ of the combined warp (not of a single mode), since the line of nodes is close to $\phi = 0$ and well covered by these samples. In the presence of both $m = 1$ and $m = 2$ modes, i.e. for a lopsided warp, such measurement can in principle obtain anything between the precession rates of these modes, i.e. $\Omega_\phi - \Omega_z \leq \dot{\phi}_{\text{lon}} \leq \Omega_\phi + \frac{1}{2}\Omega_z$, depending on their phases and relative amplitudes.

A warp can be excited either abruptly by galactic interaction(s) or gently by the continued accretion of misaligned material, which either directly forms the warp or generates an external torque that subsequently causes the warp. In the latter case, the warp tends to be dominated by the ‘simple’ $m = 1$ mode (e.g. Ostriker & Binney 1989; Shen & Sellwood 2006) at all times. In the former case of a more abrupt excitation, all modes are initially excited. Over time, all but the ‘simple’ $m = 1$ mode decay, resulting in a flaring of the warped disc (Poggio et al. 2021; Moetazedian et al., in preparation). In the transient phase during this decay, the actual line of nodes propagates in an erratic way (in fact there may be more than two nodes) where periods with $\dot{\phi}_{\text{lon}} > 0$ and $\dot{\phi}_{\text{lon}} < 0$ alternate, even if in the long term the average precession is retrograde (e.g. fig. 7 of Moetazedian et al., in preparation).

The situation is more complex for gaseous warps, for which the hydrodynamical forces may result in a faster decay to the simple warp. Since the Cepheids have only been born from the gas about one half orbital period ago, their warp should largely reflect that of the gas.

5 CONCLUSION

We have analysed the sample of all Milky Way classical optical Cepheids with *Gaia* DR3 radial velocity in terms of the Galactic warp. Unlike most previous studies, our analysis avoids fitting parametrized warp profiles, but instead we separate stars into bins according to their guiding-centre radius R_g , which is generally a better indicator of the star’s typical Galactocentric radius than its actual instantaneous radius. Our main results are as follows:

(i) At $R_g \lesssim 11$ kpc, the individual orbital planes, defined as normal to the Cepheid’s angular-momentum vectors, are on average flat, i.e. not warped. This is in contrast to some warping by 1° obtained by fitting an inclined plane to the positions, which we suggest is caused by dust obscuration.

(ii) At $R_g \gtrsim 11$ kpc, both the angular-momentum analysis and the fitted inclined planes show a warp with an amplitude of 3° – 4° . The line of nodes twists in the direction of rotation from $\phi_{\text{lon}} = -15^\circ$ at 12 kpc to 45° at 16.5 kpc. This is well described by a linear increase and corresponds to a leading spiral, adhering to Briggs’ rule for spiral galaxies. This result is not entirely novel, but our detection of the twist is much clearer than from previous studies (Chen et al. 2019).

(iii) We also determine the rate of change of the inclined planes fitted to the Cepheid positions. We find no significant time derivative for the inclination (warp amplitude), but a clear signal for $\dot{\phi}_{\text{lon}}$, the nodal precession rate of the inclined planes. We find $\dot{\phi}_{\text{lon}} = (12.4 \pm 1.6) \text{ km s}^{-1} \text{ kpc}^{-1}$ at $R_g = 12$ kpc, which broadly agrees

with previous estimates from older stars. We also find $\dot{\phi}_{\text{lon}}$ to decrease radially to $(5.9 \pm 1.3) \text{ km s}^{-1} \text{ kpc}^{-1}$ at $R_g = 14 \text{ kpc}$ and to remain roughly at this level beyond that. These values are unexpected for an ordinary warp corresponding to an inclined disc in near-circular motion, for which $\dot{\phi}_{\text{lon}} < 0$. When acting over $\sim 100 \text{ Myr}$, this measured differential precession would unwind the leading spiral of nodes, strongly suggesting that the instantaneous prograde precession is only transient and that the Milky Way warp is more complex.

For a warp excited by satellite interactions, Moetazedian et al. (in preparation) find significant fluctuations in the warp ϕ_{lon} (and hence by implication $\dot{\phi}_{\text{lon}}$), which spike in amplitude after each interaction and subsequently decline. This suggests that the measured $\dot{\phi}_{\text{lon}} > 0$ relates to a recent interaction, most likely with the Sgr dwarf galaxy, the only recent close interactor of the Milky Way.

ACKNOWLEDGEMENTS

We are grateful to R. Drimmel and S. Khanna for providing the ages and distances of classical Cepheids from G22. We thank Richard Anderson for providing his improved Cepheid period–luminosity relation prior to publication. We appreciate insightful discussions with Lia Athanassoula, Andreas Just, Peter Berczik, and Hossam Aly, and thank the reviewer, R. Drimmel, for a prompt and useful report. This work was supported by STFC grant ST/S000453/1. RS thanks the Royal Society for generous support via a University Research Fellowship. This work has made use of data from the European Space Agency (ESA) mission *Gaia* (<https://www.cosmos.esa.int/gaia>), processed by the *Gaia* Data Processing and Analysis Consortium (DPAC; <https://www.cosmos.esa.int/web/gaia/dpac/consortium>). Funding for the DPAC has been provided by national institutions, in particular the institutions participating in the *Gaia* Multilateral Agreement.

DATA AVAILABILITY

No data were generated in this study.

REFERENCES

- Anderson R. I., Ekström S., Georgy C., Meynet G., Mowlavi N., Eyer L., 2014, *A&A*, 564, A100
- Anderson R. I., Saio H., Ekström S., Georgy C., Meynet G., 2016, *A&A*, 591, A8
- Binney J. J., Tremaine S., 2008, *Galactic Dynamics*, 2nd edn. Princeton Univ. Press, Princeton, NJ
- Bosma A., 1991, in Casertano S., Sackett P. D., Briggs F. H., eds, *Warped Disks and Inclined Rings Around Galaxies*. Cambridge Univ. Press, Cambridge, p. 181
- Breuval L., Riess A. G., Kervella P., Anderson R. I., Romaniello M., 2022, *ApJ*, 939, 89
- Briggs F. H., 1990, *ApJ*, 352, 15
- Burke B. F., 1957, *AJ*, 62, 90
- Burton W. B., 1988, in Kellermann K. I., Verschuur G. L., eds, *Galactic and Extragalactic Radio Astronomy*. Springer-Verlag, Berlin, p. 295
- Chen X., Wang S., Deng L., de Grijs R., Liu C., Tian H., 2019, *Nat. Astron.*, 3, 320
- Cheng X. et al., 2020, *ApJ*, 905, 49
- Chrobáková Ž., López-Corredoira M., 2021, *ApJ*, 912, 130
- Chrobáková Ž., Nagy R., López-Corredoira M., 2022, *A&A*, 664, A58
- Cruz Reyes M., Anderson R. I., 2023, *A&A*, 672, A85
- Dehnen W., 1998, *AJ*, 115, 2384
- Djorgovski S., Sosin C., 1989, *ApJ*, 341, L13
- Drimmel R., Spergel D. N., 2001, *ApJ*, 556, 181
- Drimmel R., Smart R. L., Lattanzi M. G., 2000, *A&A*, 354, 67
- Freudenreich H. T. et al., 1994, *ApJ*, 429, L69
- Gaia Collaboration, 2022a, *A&A*, <https://doi.org/10.1051/0004-6361/202243797>
- Gaia Collaboration, 2022b, *A&A*, <https://doi.org/10.1051/0004-6361/202243940>
- García-Ruiz I., Sancisi R., Kuijken K., 2002, *A&A*, 394, 769
- Henderson A. P., Jackson P. D., Kerr F. J., 1982, *ApJ*, 263, 116
- Inno L., Rix H.-W., Stanek K. Z., Jayasinghe T., Poggio E., Drimmel R., Rotundi A., 2021, *ApJ*, 914, 127
- Johnston K. V., Hernquist L., Bolte M., 1996, *ApJ*, 465, 278
- Kervella P. et al., 2019, *A&A*, 623, A117
- Lemasle B. et al., 2022, *A&A*, 668, A40
- Levine E. S., Blitz L., Heiles C., 2006, *ApJ*, 643, 881
- Li C., Binney J., 2022, *MNRAS*, 516, 3454
- Li X. Y., Huang Y., Chen B. Q., Wang H. F., Sun W. X., Guo H. L., Li Q. Z., Liu X. W., 2020, *ApJ*, 901, 56
- Lindgren L. et al., 2021, *A&A*, 649, A2
- López-Corredoira M., Cabrera-Lavers A., Garzón F., Hammersley P. L., 2002, *A&A*, 394, 883
- López-Corredoira M., Abedi H., Garzón F., Figueras F., 2014, *A&A*, 572, A101
- Nelson D. et al., 2019, *MNRAS*, 490, 3234
- Ostriker E. C., Binney J. J., 1989, *MNRAS*, 237, 785
- Pietrukowicz P. et al., 2015, *ApJ*, 813, L40
- Pietrukowicz P., Soszyński I., Udalski A., 2021, *Acta Astron.*, 71, 205
- Pillepich A. et al., 2019, *MNRAS*, 490, 3196
- Poggio E. et al., 2018, *MNRAS*, 481, L21
- Poggio E., Drimmel R., Andrae R., Bailer-Jones C. A. L., Fournesneau M., Lattanzi M. G., Smart R. L., Spagna A., 2020, *Nat. Astron.*, 4, 590
- Poggio E. et al., 2021, *A&A*, 651, A104
- Reylé C., Marshall D. J., Robin A. C., Schultheis M., 2009, *A&A*, 495, 819
- Ripepi V., Molinaro R., Musella I., Marconi M., Leccia S., Eyer L., 2019, *A&A*, 625, A14
- Ripepi V. et al., 2022a, *A&A*, <https://doi.org/10.1051/0004-6361/202243990>
- Ripepi V. et al., 2022b, *A&A*, 659, A167
- Romero-Gómez M., Mateu C., Aguilar L., Figueras F., Castro-Ginard A., 2019, *A&A*, 627, A150
- Sánchez-Saavedra M. L., Battaner E., Florido E., 1990, *MNRAS*, 246, 458
- Schönrich R., 2012, *MNRAS*, 427, 274
- Schönrich R., Dehnen W., 2018, *MNRAS*, 478, 3809
- Schönrich R., Binney J., Dehnen W., 2010, *MNRAS*, 403, 1829
- Schönrich R., Asplund M., Casagrande L., 2011, *MNRAS*, 415, 3807
- Semczuk M., Dehnen W., Schönrich R., Athanassoula E., 2023, *MNRAS*, 519, 902
- Shen J., Sellwood J. A., 2006, *MNRAS*, 370, 2
- Skowron D. M. et al., 2019a, *Acta Astron.*, 69, 305
- Skowron D. M. et al., 2019b, *Science*, 365, 478
- Wang H. F. et al., 2020, *ApJ*, 897, 119
- Westerhout G., 1957, *Bull. Astron. Inst. Neth.*, 13, 201
- Williams M. E. K. et al., 2013, *MNRAS*, 436, 101

This paper has been typeset from a \LaTeX file prepared by the author.